Memorias del Congreso Nacional de Control Automático
ISSN: 2594-2492

# Diagnosis Strategy for a Faulty Leg in the H-Bridge of CHB-$n$L Converters

**K.O. Mtepele, D.U. Campos-Delgado, A.A. Valdez-Fernández**

**Abstract:** This research paper proposes a diagnosis scheme for open circuit faults (OCFs) in the whole leg of cascaded H-bridge converters with $n$-levels (CHB-$n$L). This work considers a single-phase operation of the CHB-$n$L converter with a shunt active filter application. The fault detection and isolation goal is accomplished by analyzing the capacitor current in each H-bridge. Our analysis shows that this current is always non-negative after a faulty leg condition. So to avoid extra measurements, a low-pass filtered version of each capacitor voltage is employed to compute the residual. The residuals provide specific characteristics that allow to detect and isolate the faulty leg in the CHB-$n$L converter without the necessity of using additional sensors. The proposed diagnosis strategy is validated in simulation with a CHB-7L topology, with different faulty legs scenarios and a load disturbance test.

*Keywords:* Fault diagnosis, open-circuit faults, multilevel converter.

## 1. INTRODUCTION

Nowadays the usages of power electronic components are increasing significantly in the household and industrial applications due to the advancement in the control strategies. The non-linear loads connected to these systems introduce harmonics into the power system network. These harmonics increase the losses and reduce the lifetime of the power system equipments (Peng et al., 1990). Therefore, the amount of harmonics injected to the network should be minimized for power quality improvement. This objective could be achieved by introducing active power filters (APF), among others solutions (Valdez et al., 2013). Cascaded H-bridge (CHB) multilevel converters are used in the implementation of APFs. The popularity of these converters has been due to several structural and operational advantages, including the following: (i) their modular design with a simplified structure; (ii) the availability of control strategies to balance the DC voltages in the H-bridges; (iii) the quality of the output voltage can be adjusted by the number of cascaded H-bridges in the converter (Kouro et. al., 2011; Gultekin , 2012).

In this context, novel APFs rely on the advantages of multilevel topologies to achieve a high performance, but at the expense of a large number of semiconductor devices. Nonetheless, the probability of a fault in multilevel converters is raised by the number of semiconductors employed in the topology (Mirafzal, 2014). In Choi et al. (2015) and many other works, a high percentage of faults has been reported in the switching devices of the multilevel converters, which can be classified in two groups: open-circuit faults (OCFs), and short-circuit ones (SCFs). However, passive devices (fuses) can be added to the power switches in order to convert SCFs to OCFs. This strategy allows to treat both types of faults by the same electrical symptoms and similar diagnostic algorithms (Wang et al., 2015). Thus, in multilevel converters, there is a great interest on detecting and isolating the OCFs in the power switches. In addition, an efficient diagnostic strategy can reduce the downtime cost of industrial power electronics systems. More importantly, the information of the identified faulty switches in the multilevel converters can be utilized to trigger the corresponding fault-tolerant operation strategy for safety-critical applications (Zhendong et al., 2014).

For the case of OCFs, in Shunfeng et. al. (2017), a diagnosis method for modular multilevel converters was proposed in a distributed control architecture, which makes the local controllers capable of identifying the faults in the switching devices. From which, instead of using the capacitor voltage measurement, the sub-module terminal voltage is measured for capacitor voltage control and fault diagnosis according to different sampling instances. In addition, many solutions have been proposed (Mirafzal, 2014) - (Ouni et al., 2015). Specifically, Mirafzal (2014) gives a detailed review of published fault detection techniques, while Choi et al. (2015) provide an overview of the failure mechanisms in IGBTs modules and their handling methods. Meanwhile, a fault diagnosis and fault tolerant method for SCF in cascaded half-bridge inverters based on a model-based approach was suggested in Alavi et al. (2015). In Ouni et al. (2015), a method to detect the faulty cell in a CHB inverter was suggested by comparing the output voltage with the reference one, synthesized by the control states of the switches and DC-link voltage. In Shu et al. (2016), a fast detection is reached with the help of additional sensors, but this solution increases the system complexity and cost. Recently, observer model-based methods have been proposed for FDI purposes (An et al., 2016) - (Jlassi et al., 2016), where well-known techniques such as Luenberger state observers, nonlinear observers, or proportional-integral observers were employed. In fact, our previous research work in Mtepele et al. (2017) relied on these methods, because they achieve an efficient diagnosis scheme with a relatively short detection time, which is a crucial factor in the correct operation of CHB converters. However, this strategy could not address a case of simultaneous faults triggered in the whole leg/branch of an individual H-bridge of the CHB converter, which

 

is relevant in practical applications due to the use of commercial gate drivers for the switching devices.

In this context, this work proposes a solution to the undetermined case encountered in our previous contribution (Mtepele et al., 2017), thereby a fault detection and isolation (FDI) strategy is studied for OCFs in the whole leg of each H-bridge in single-phase $n$-level CHB converters (CHB-$n$L). In the present paper, the capacitor current in each H-bridge of the CHB-$n$L converter is analyzed to detect and isolate the simultaneous OCFs of the same leg. But to avoid extra sensors, the residuals are built based on the derivative of low-pass versions of the capacitor voltages. To validate the proposed FDI strategy, we present an evaluation based on numerical simulations for different faulty legs, where we also consider a robustness test under load perturbations.

The rest of the paper is organized with the following structure. Section 2 provides a brief description of the single-phase CHB-$n$L converter used in this work, and also introduces the mathematical model and the control philosophy for the shunt APF operation. The proposed FDI scheme is motivated and detailed in Section 3. Section 4 shows the evaluation of the proposal in a single-phase CHB topology with seven-levels, and finally concluding remarks are described in Section 5.

## 2. CHB-$n$L CONVERTER

Figure 1 shows the general structure of the studied single-phase CHB-$n$L converter topology used as shunt APF (SAPF) in this research work. The corresponding generalized model of the system represented in this figure can be obtained by the application of Kirchhoff's law, which yields the following model of the system dynamics:

$$i_S = i + i_0 \tag{1}$$

$$L\frac{d}{dt}i = v_S - \sum_{j=1}^{N} u_j v_{Cj}, \tag{2}$$

$$C\dot{v}_{Cj} = u_j i - \frac{1}{R}v_{Cj} \quad j \in [1, N] \tag{3}$$

where $N$ indicates the total number of H-bridges in the converter that generate $n = 2N + 1$ voltage levels, $v_S$ denotes the voltage at the point of common coupling (PCC), also referred to as the grid voltage, $i_S$ is the grid current, $i$ is the injected current, $i_0$ is the distorted load current consumed by a nonlinear load; $v_{Cj}$ is the capacitor voltage in the DC-bus of the $j$-th H-bridge, and $u_j \in \{-1, 0, 1\}$ represents the switch position for the $j$-th H-bridge and plays the role of the actual control input. The four switches in the $j$-th H-bridge are denoted as $(Q_{j1}, \bar{Q}_{j1}, Q_{j2}, \bar{Q}_{j2})$ (see Fig. 1). The electric parameters in the SAPF are $L$ as the input inductor, $C$ the capacitance in the DC bus and $R$ the associated discharge resistance (assumed both equal in all H-bridges). The operation of the $j$-th H-bridge is described as follows:

**a)** if $u_j = 1$, then power switches $(Q_{j1}$ & $\bar{Q}_{j2}) \rightarrow$ ON, while $(\bar{Q}_{j1}$ & $Q_{j2}) \rightarrow$ OFF,
**b)** if $u_j = -1$, then power switches $(\bar{Q}_{j1}$ & $Q_{j2}) \rightarrow$ ON, while $(Q_{j1}$ & $\bar{Q}_{j2}) \rightarrow$ OFF,
**c)** If $u_j = 0$, $Q_{j1}$ & $Q_{j2}$ (or $\bar{Q}_{j1}$ & $\bar{Q}_{j2}$) are simultaneously switched on.

An averaged model is considered instead of the above described switching model for control design purposes. For this aim, and from now on, the switch positions $(u_1, \ldots, u_N)$ represent duty cycles, i.e., they are considered continuous signals limited to the interval $[-1, 1]$, rather than in the discrete set $\{-1, 0, 1\}$. This scenario is based on the assumption that, in a real-time implementation, the effects of the switching frequency on the DC-link voltage of each H-bridge are filtered out by its corresponding capacitor. The induced voltaje by the $j$-th H-bridge is then represented as $e_j = u_j v_{Cj}$. For more details on the mathematical modelling, the reader may refer to Valdez et al. (2015).

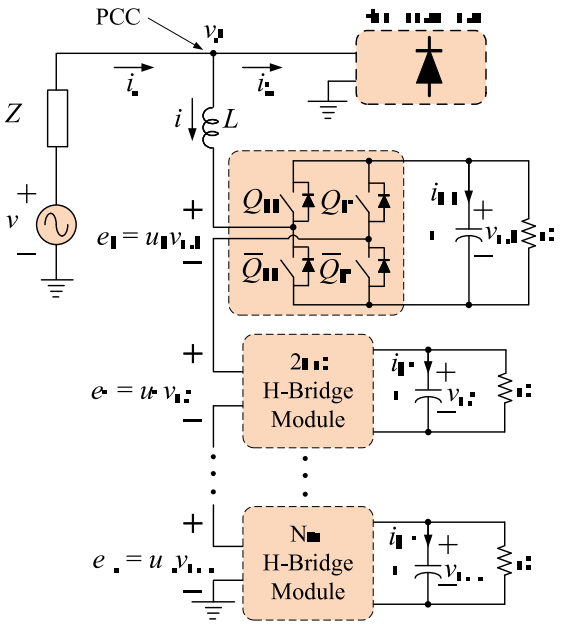


Fig. 1. Single-phase CHB-$n$L converter used as shunt APF.

From the previous average model, a nominal controller for the shunt APF operation was presented in Valdez et al. (2015), which consists of three feedback loops: a current tracking loop, a voltage regulation loop, and $N-1$ voltage balance loops. The current tracking loop is composed by a proportional term related to the tracking error, plus a bank of harmonic oscillators tuned at the harmonics of interest to guarantee performance. For this purpose, a current reference $i_S^*$ proportional to the fundamental component of the source voltage $v_S$ is constructed to provide an almost pure sinusoidal source current $i_S$. The voltage regulation loop is based on a conventional *PI* controller with a limited bandwidth, so that the DC buses in each H-bridges is fixed, in average, at a constant value $V_d$. There are $N - 1$ voltage balance loops which are synthesized as amplitude-modulated signals proportional to the fundamental component of the source voltage $v_S$, where the modulating gains are also obtained by conventional *PI* control laws. In this work, the injected current $i$, and the voltages in the H-bridges $(v_{C1}, \ldots, v_{CN})$ are assumed known variables in the control and fault diagnosis methodologies.

 

## 3. FAULT DIAGNOSIS STRATEGY

As previously stated, this work deals with the diagnosis strategy of a faulty leg in the H-bridge of single-phase CHB-$n$L converters. During the implementation of CHB-$n$L converters, gate drivers are used to activate each leg in the H-bridge, so in the case of a faulty gate driver, the whole leg will be inactive. So, the condition of a simultaneous OCFs in a leg of the H-bridge is of practical relevance. In Mtepele et al. (2016) and Mtepele et al. (2017), the system described by expressions (2)-(3) was employed to construct a sliding-mode observer in a model-based FDI proposal, and this observer was used for the detection and isolation of the OCFs in the switching devices of the CHB-$n$L converter. From which, only the measurements of the injected current $i$ and capacitor voltages $(v_{C1}, \ldots, v_{CN})$ were necessary to implement the diagnosis media. When it comes to the faults in the whole leg of the $j$-th H-bridge, i.e. simultaneous faults in switches $(Q_{j1}$ & $\bar{Q}_{j1})$ or $(Q_{j2}$ & $\bar{Q}_{j2})$, the above strategy becomes incomplete because, during this scenario, the induced fault profiles are alternating between negative and positive values (Mtepele et al., 2016)- (Mtepele et al., 2016); and since the proposed nonlinear observers estimate the DC component of the induced fault profiles, the resulting residuals are not significant.

To overcome the problem mentioned above, the capacitor current signal $i_{Cj}$ of the $j$-th H-bridge is analyzed to handle the diagnosis procedure by recalling that in a nominal condition, this current has an alternated time-profile. Hence after a faulty leg, the capacitor current in the damaged H-bridge can only flow in one direction through the anti-parallel diodes, and consequently, this signal can only be equal or greater than zero. To justify this conclusion, take as example the first H-bridge $(j = 1)$ shown in Fig. 1:

- Faulty leg $(Q_{11}$ & $\bar{Q}_{11})$:
  **(a)** if $i > 0$ & $Q_{12} \rightarrow$ OFF $\Rightarrow e_1 = v_{C1}$,
  **(b)** if $i > 0$ & $Q_{12} \rightarrow$ ON $\Rightarrow e_1 = 0$,
  **(c)** if $i < 0$ & $Q_{12} \rightarrow$ OFF $\Rightarrow e_1 = 0$,
  **(d)** if $i < 0$ & $Q_{12} \rightarrow$ ON $\Rightarrow e_1 = v_{C1}$.
- Faulty leg $(Q_{12}$ & $\bar{Q}_{12})$:
  **(a)** if $i < 0$ & $Q_{11} \rightarrow$ OFF $\Rightarrow e_1 = v_{C1}$,
  **(b)** if $i < 0$ & $Q_{11} \rightarrow$ ON $\Rightarrow e_1 = 0$,
  **(c)** if $i > 0$ & $Q_{11} \rightarrow$ OFF $\Rightarrow e_1 = 0$,
  **(d)** if $i > 0$ & $Q_{11} \rightarrow$ ON $\Rightarrow e_1 = v_{C1}$.

by recalling that $(Q_{12}$ & $\bar{Q}_{12})$, and $(Q_{11}$ & $\bar{Q}_{11})$ are complementary power switches. Furthermore, by the non-negative capacitor current $i_{C1} \geq 0$, an increment in the capacitor voltage $v_{C1}$ will be induced as a result of the faulty leg. Meanwhile, due to the closed-loop strategy in the SAPF which always aim to regulate and balance these voltages in each CHB-$n$L converter, the remaining capacitor voltages will tend to decrease. Figure 2 illustrates the resulting time-profiles of the capacitor current $i_{C1}$ during simultaneous faults in the first H-bridge for the first and second legs, i.e. $(Q_{11}$ & $\bar{Q}_{11})$ and $(Q_{12}$ & $\bar{Q}_{12})$.

In fact, this described pattern will be distinctive of a faulty leg independently of the other studied single and simultaneous OCFs. To avoid using extra sensors, and since just the trend in the $j$-th capacitor current is

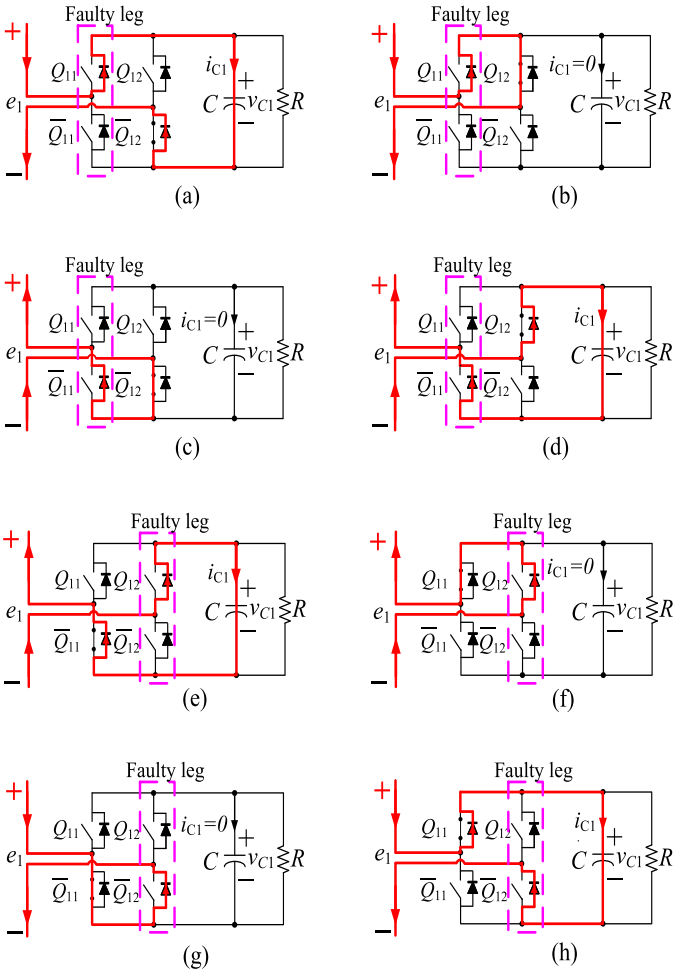


Fig. 2. Time-profile of the capacitor current $i_{C1}$ during simultaneous faults in first H-bridge; in the first leg $(Q_{11}$ & $\bar{Q}_{11})$ represented by subfigures (a), (b), (c), and (d); in the second leg $(Q_{12}$ & $\bar{Q}_{12})$ illustrated by (e), (f), (g) and (h).

required, the residual signal $d\hat{v}_{Cj}/dt$ is used for diagnosis purposes, where $\hat{v}_{Cj}$ is a low-pass filtered version of the measurement $v_{Cj}$. Furthermore, by recalling that a fault in legs $(Q_{j1}$ & $\bar{Q}_{j1})$ or $(Q_{j2}$ & $\bar{Q}_{j2})$ of the $j$-th H-bridge will always cause a positive capacitor current, the corresponding effect is a decrement of the other capacitor currents in the healthy H-bridges that will help to isolate this kind of fault. Mathematically, the detection can be achieved by evaluating $d\hat{v}_{Cj}/dt$, in such a way that

$$r_{Cj} \triangleq \frac{d}{dt}\hat{v}_{Cj} > I_{TH}, \tag{4}$$

with $j \in \{1, \ldots, N\}$.

In specific for the CHB-$n$L converter with $N = 3$, the diagnosis strategy is given by

- $Q_{11}$ & $\bar{Q}_{11}$ (1st H-bridge)
  $(r_{C1} > r_{C3})$ & $(r_{C3} > r_{C2})$ & $(r_{C1}, r_{C3}) > I_{TH}$ (5)
- $Q_{12}$ & $\bar{Q}_{12}$ (1st H-bridge)
  $(r_{C1} > r_{C2})$ & $(r_{C2} > r_{C3})$ & $(r_{C1}, r_{C2}) > I_{TH}$ (6)
- $Q_{21}$ & $\bar{Q}_{21}$ (2nd H-bridge)
  $(r_{C2} > r_{C3})$ & $(r_{C3} > r_{C1})$ & $(r_{C2}, r_{C3}) > I_{TH}$ (7)
- $Q_{22}$ & $\bar{Q}_{22}$ (2nd H-bridge)

$$(r_{C2} > r_{C1}) \;\&\; (r_{C1} > r_{C3}) \;\&\; (r_{C1}, r_{C2}) > I_{TH} \quad (8)$$

- $Q_{31}$ & $\bar{Q}_{31}$ (3rd H-bridge)

$$(r_{C3} > r_{C2}) \;\&\; (r_{C2} > r_{C1}) \;\&\; (r_{C2}, r_{C3}) > I_{TH} \quad (9)$$

- $Q_{32}$ & $\bar{Q}_{32}$ (3rd H-bridge)

$$(r_{C3} > r_{C1}) \;\&\; (r_{C1} > r_{C2}) \;\&\; (r_{C1}, r_{C3}) > I_{TH} \quad (10)$$

where $I_{TH}$ is a detection threshold, which is selected by considering the measurement noise in the capacitor voltages.

## 4. SIMULATION RESULTS

In order to evaluate the OCF diagnosis strategies addressed in this work, a simulation test of a single-phase SAPF based on a seven-levels CHB (CHB-7L) topology with $N = 3$ H-bridges is performed in the present section. The employed parameters during the evaluation stage are: rms value of the source voltage 127 $V_{RMS}$, nominal frequency $f_0 = 60$ Hz, inductance of SAPF $L = 3.6$ mH and the capacitances in each H-bridge $C = 2000$ $\mu$F. The nonlinear load is represented by a full-wave rectifier that includes a smoothing inductor of $L_0 = 0.1$ mH, DC capacitor $C_0 = 87$ $\mu$F, and output nominal resistance $R_0 = 50$ $\Omega$. The discrete-controller scheme has been implemented in Simulink/MATLAB, with a sampling frequency of $f_s = 40$ kHz. During the evaluation, two cases are considered: i). a faulty leg condition, and (ii). a load disturbance (step changes in the load resistor $R_0$ of the rectifier).

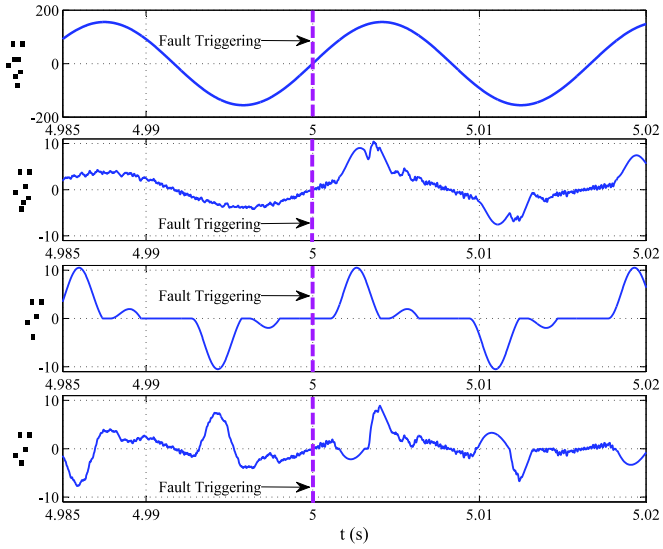


Fig. 3. Pre and post fault operation with ($Q_{11}$ & $\bar{Q}_{11}$) OCF in 1st H-bridge: (top) voltage source $v_S$, (middle-top) source current $i_S$, (middle-bottom) load current $i_0$, (bottom) injected current $i$.

### *4.1 Faulty Leg Condition*

At first, the single-phase CHB-7L converter is evaluated in closed-loop under the proposed control scheme for a nominal condition. Next, the proposed FDI scheme is considered under faulty legs in 1st H-bridge. Figure 3 shows from top to bottom, source voltage $v_S$, source current $i_S$, load current $i_0$ and the injected current $i$ before and after the occurrence of a faulty leg ($Q_{11}$ & $\bar{Q}_{11}$) at $t = 5$ s. Notice that the compensated source current $i_S$ is almost a pure sinusoidal signal, which is in-phase with the source voltage $v_S$ despite the highly distorted load current $i_0$. This observation implies that the SAPF injects an appropriate current $i$, such that $i_S$ has good tracking over its reference. Meanwhile, Fig. 4 illustrates that the capacitor voltages ($v_{C1}, v_{C2}, v_{C3}$) (top to bottom) are regulated before the OCFs scenario. After the OCF is induced in any of the H-bridges of the CHB-7L converter, an induced distortion is highlighted in the currents and voltages, as shown in Figs. 3 and 4.

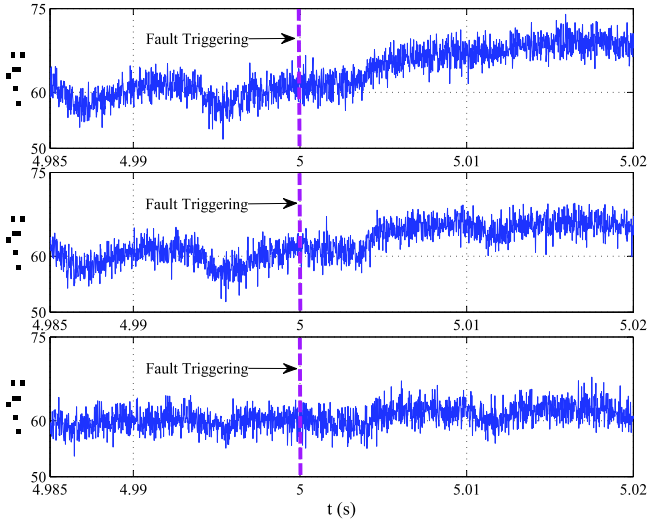


Fig. 4. Pre and post fault operation with ($Q_{11}$ & $\bar{Q}_{11}$) OCF in 1st H-bridge: (top) First capacitor voltage $v_{C1}$, (middle) second capacitor voltage $v_{C2}$, (bottom) third capacitor voltage $v_{C3}$.

Next, Fig. 5 shows the time responses of the residuals ($r_{C1}, r_{C2}, r_{C3}$) before and after fault triggering. Notice that the FDI condition in (5) is reached, so this situation indicates the OCF in the first leg of the first H-bridge (i.e., $Q_{11}$ & $\bar{Q}_{11}$, see Fig. 1). On the other hand, Fig. 6 presents

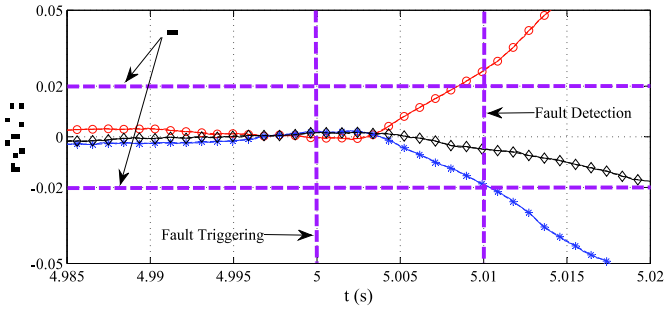


Fig. 5. Residuals $r_{C1}$ ($\circ$),$r_{C2}$ ($\diamond$) and $r_{C3}$ ($*$), during OCFs in switches ($Q_{11}$ & $\bar{Q}_{11}$) at $t = 5$ $s$.

the time-profile of the residual signals ($r_{C1}, r_{C2}, r_{C3}$) after OCFs in the second leg of the first H-bridge (i.e., $Q_{12}$ & $\bar{Q}_{12}$, see Fig. 1). Observe that now the residuals satisfy the expression (6) after fault triggering. In addition to that, Table 1 illustrates the detection time ($ms$) for different faulty legs in the CHB-7L converter. Consequently, the detection time is always lower than one cycle of the supply voltage.

### *4.2 Load Disturbance*

Figure 7 shows the robustness of the signals $(r_{C1}, r_{C2}, r_{C3})$ during the presence of load perturbations. This evaluation was conducted by a step change in the resistance located of the full-wave rectifier used as load in the SAPF, from $R_0 = 50\ \Omega$ to $100\ \Omega$ at $t = 5.0\ s$, and then back to $R_0 = 50\ \Omega$ at $t = 5.5\ s$. As expected, the transient in the residuals did not exceed the detection threshold $I_{TH}$, so good robustness is highlighted.

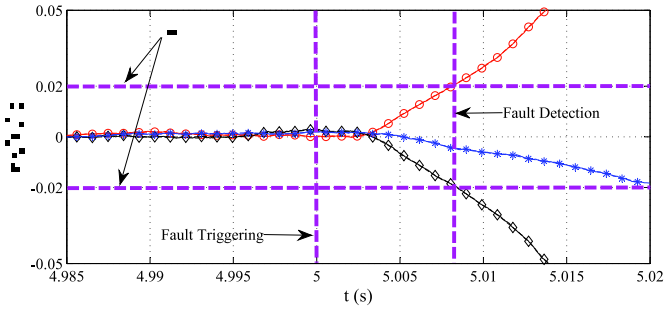


Fig. 6. Residuals $r_{C1}$ $(\circ)$, $r_{C2}$ $(\diamond)$ and $r_{C3}$ $(*)$, during OCFs in switches $(Q_{12}$ & $\bar{Q}_{12})$ at $t = 5\ s$.

Table 1. Detection time for a faulty leg during the simulation evaluation.

| OCF Type | Time $(ms)$ |
|---|---|
| $Q_{11}$ & $\bar{Q}_{11}$ | 9.4 |
| $Q_{12}$ & $\bar{Q}_{12}$ | 8.2 |
| $Q_{21}$ & $\bar{Q}_{21}$ | 8.5 |
| $Q_{22}$ & $\bar{Q}_{22}$ | 7.9 |
| $Q_{31}$ & $\bar{Q}_{31}$ | 8.6 |
| $Q_{32}$ & $\bar{Q}_{32}$ | 7.8 |

Note: a cycle of $v_S$ represents 16.66 $ms$

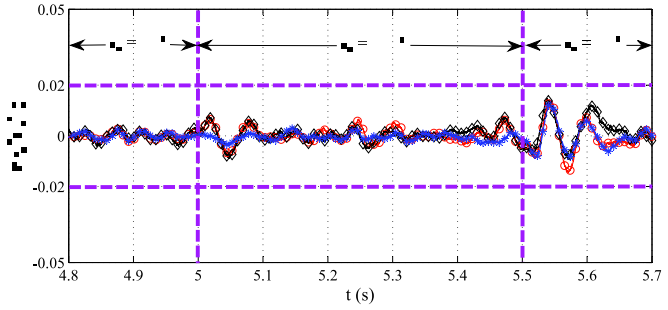


Fig. 7. Residuals $r_{C1}$ $(\circ)$,$r_{C2}$ $(\diamond)$ and $r_{C3}$ $(*)$, during step changes in $R_0$ at $t \approx 5\ s$ to $t \approx 5.5\ s$.

## CONCLUDING REMARKS

This work presented the diagnosis strategy for a faulty leg in the H-bridge of single-phase CHB-$n$L converters used as SAPF. In order to accomplish this goal, the time-profile of the capacitor currents in the H-bridges was analyzed. An important property of the present research work is that the diagnosis media was carried out without the need of additional sensors and the information of the system model. To validate the ideas proposed in this work, a simulation study was conducted under different faulty leg OCF scenarios. During the evaluation process, the residuals only required less than one cycle of the fundamental frequency $f_0$ to detect a fault throughout the studied scenarios. Moreover, the residuals also showed good robustness against load disturbances. In future work, the proposed diagnosis scheme will be validated experimentally in single and three-phase versions of the CHB-$n$L converter. Furthermore, qualitative and quantitative guidelines for the selection of the detection threshold $I_{TH}$ will be studied, indicated in expressions (5)-(10).

## REFERENCES


F. Z. Peng, H. Akagi, G. Escobar, and A. Nabae, A new approach to harmonic compensation in power systems-a combined system of shunt passive and series active filters *IEEE Trans. on Ind. Appl.*, 26:983-990, 1990.

A. A. Valdez-Fernández, P. R. Martínez-Rodríguez, G. Escobar, C. A. Limones-Pozos, and J. M. Sosa, A Model-Based Controller for the Cascade H-Bbridge Multilevel Converter Used as a Shunt Active Filter. *IEEE Trans. Ind. Electron.*, 60:5019-5028, 2013.

B. Mirafzal, Survey of Fault-Tolerance Techniques for Three-Phase Voltage Source Inverters. *IEEE Trans. Ind. Electron.*, 61:5192-5201, 2014.

Shunfeng Yang, Yi Tang and Peng Wang Open-circuit fault diagnosis of switching devices in a modular multilevel converter with distributed control. *2017 IEEE Energy Conversion Congress and Exposition (ECCE)*, 4208-4214, 2017.

U.M. Choi, F. Blaabjerg, and K. B. Lee, Study and Handling Methods of Power IGBT Module Failures in Power Electronic Converter Systems. *IEEE Trans. Pow. Electron.*, 30:2517-2533, 2015.

Z. Ji, J. Zhao, Y. Sun, X. Yao, and Z. Zhu, Fault-Tolerant Control of Cascaded H-Bridge Converters Using Double Zero-Sequence Voltage Injection and DC Voltage Optimization. *Journal of Power Electron.*, 14:946-956, 2014.

C. Shu, C. Ya-Ting, Y. Tian-Jian, and W. Xun, A novel diagnostic technique for open-circuited faults of inverters based on output line-to-line voltage model. *IEEE Trans. Ind. Electron.*, 63:4412-4421, Jul. 2016.

Q. T. An, L. Sun, and L. Z. Sun, Current residual vector-based openswitch fault diagnosis of inverters in PMSM drive systems. *IEEE Trans. Ind. Electron.*, 30:2814-2827, May. 2015.

I. Jlassi, J. O. Estima, S.K. El Khil, N. M. Bellaaj, and A. J. M. Cardoso, Multiple open-circuit faults diagnosis in back-to-back converters of PMSG drives for wind turbine systems. *IEEE Trans. Ind. Electron.*, 30:2689-2702, May. 2015.

K. O. Mtepele, D. U. Campos-Delgado, A. Valdez-Fernandez and J. A. Pecina-Snchez, Fault tolerant controller for a generalized n-level CHB multilevel converter. *13th Int. Conf. on Power Electronics (CIEP)*, 75-80, Guanajuato, MX, 2016.

K.O Mtepele, J. A. Pecina-Sánchez, D.U Campos-Delgado and A. A. Valdez-Fernández, Open Circuit Fault Diagnosis Strategy for a Generalized $n$-Levels CHB Multilevel Converter, *Congreso Nacional de Control Automático (CNCA)*, 205-210, Queretaro, MX, 2016.

K.O Mtepele, D.U Campos-Delgado and A. A. Valdez-Fernández, J. A. Pecina-Sánchez, Fault Diagnosis for


 

Generalized $n$-Levels 3-Phase CHB Multilevel Converters, *Congreso Nacional de Control Automático (CNCA)*, 14-19, Nuevo Leon, MX, 2017.

M. Alavi, D. Wang, and M. Luo, Model-based Diagnosis and Fault Tolerant Control for Multi-Level Inverters. *In Proc. IECON 2015*, 1548-1553, Yokohama, Japan, 2015.

S. Ouni, J. Rodriguez, *et al.*, A Fast and Simple Method to Detect Short Circuit Fault in Cascade H-Bridge Multilevel Inverter. *In Proc. ICIT 2015*, 866-871, Seville, Spain, 2015.

A. A. Valdez-Fernández, K.O Mtepele, and D.U Campos-Delgado, A Generalized Model-Based Controller for the n-level CHB Multilevel Converter Used as a Shunt Active Filter. *IEEE Int. Autumn Meet. on Pow. Electron. and Comp. (ROPEC)*, Guerrero, MX, Nov. 2015.

T. Wang, H. Xu, J. Han, H. Bouchikhi, and M. H. Benbouzid, Cascaded H-Bridge Multilevel Inverter System Fault Diagnosis Using a PCA and Multiclass Relevance Vector Machine Approach. *IEEE Trans. Pow. Electron.*, 30:7006-7018, 2015.

S. Kouro, M. Malinowski, K. Gopakumar, J. Pou, L. G. Franquelo, B. Wu, J. Rodriguez, M. A. Prez, and J. I. Leon Recent advances and industrial applications of multilevel converters. *IEEE Trans. Pow. Electron.*, 57:2553-2580, Aug. 2010.

B. Gultekin Design and implementation of a 154-kV, 50-Mvar transmission STATCOM based on 21-level cascaded multilevel converter. *IEEE Trans. Ind. Appl.*, 48:3:1030-1045, May/Jun. 2012.

 